First-principles molecular dynamics simulation of liquid Mg_3Bi_2

1996 J. Phys.: Condens. Matter 8 1879

(http://iopscience.iop.org/0953-8984/8/12/004)

J. Phys.: Condens. Matter **8** (1996) 1879–1896. Printed in the UK

First-principles molecular dynamics simulation of liquid Mg_3Bi_2

G A de Wijs†‖, G Pastore‡, A Selloni§ and W van der Lugt†

† Solid State Physics Laboratory, University of Groningen, Nijenborgh 4, 9747 AG, Groningen, The Netherlands

‡ Dipartimento di Fisica Teorica dell' Università, Strada Costiera 11, 34014 Trieste, Italy

§ Departement de Chimie Physique, Université de Genève, 30 quai E Ansermet, CH-1211, Genève, Switzerland

Received 24 July 1995, in final form 4 October 1995

Abstract. The liquid Mg–Bi system exhibits strong compound formation at the 'octet' composition (Mg_3Bi_2). We present results of first-principles molecular dynamics simulations of this alloy system at different compositions: the pure Mg and Bi liquid components, the stoichiometric liquid, and a Mg-rich composition ($Mg_{62}Bi_{28}$). For the pure liquids, our results are in excellent agreement with experimental diffraction data. For Mg_3Bi_2, a significant modification of the characteristics of the local ordering is found w.r.t. the crystalline α-phase: the ordering in the liquid is much more ionic. This structural modification is consistent with the structure of the superionic β-phase, that was reported recently by Barnes *et al* 1994 *J. Phys.: Condens. Matter* **6** L467. Our simulations cannot reproduce the 'reverse' metal–nonmetal transition observed upon melting, the computed conductivity being much larger than found in experiments. Instead, for the Mg-rich $Mg_{62}Bi_{28}$ alloy, the calculated conductivity approaches closely to the experimental value.

1. Introduction

For various reasons the alloys of magnesium with antimony and bismuth are intriguing from a physical–chemical point of view. Seitz [1] characterizes the octet compound Mg_3Sb_2 as a transition case with properties in between those of ionic crystals and metallic alloys. A glance at the phase diagram reveals [2, 3] that the octet composition is the only composition of the Mg–Sb system for which compounds (an α- and a β-phase) are formed. They have the narrow existence ranges characteristic of ionic phases. The liquidus [2, 3] exhibits a sharp, cusp-like maximum at around the stoichiometric composition.

The phase diagram of the Mg–Bi system [4, 5] is very similar to that of Mg–Sb. The maximum temperature of the liquidus is 821 °C and is found at the octet composition. There is an α-phase up to 703 °C and a β-phase between 703 °C and 821 °C. Only few crystal structures are compatible with the composition ratio 2:3. The α-phase crystallizes in the hexagonal La_2O_3 structure [6]. The coordination of the Bi atoms is somewhat irregular: the first two Mg coordination shells together contain an odd number of atoms. According to Barnes *et al* [7] β-Mg_3Bi_2 crystallizes with the Bi atoms on a bcc lattice and is a superionic conductor with Mg^{2+} as the mobile ion.

‖ Present address: CECAM, Ecole Normale Supérieure de Lyon, 46 Allée d'Italie, 69364 Lyon Cedex 07, France.

0953-8984/96/121879+18$19.50

In spite of the apparent similarities between Mg_3Bi_2 and Mg_3Sb_2 the electrical resistivities differ widely. Stepanow [8] found that solid Mg_3Bi_2 behaves as a good metal. This was confirmed in a very detailed study by Grube *et al* [4] and is in agreement with band-structure calculations by Xu *et al* [9]. In contrast, solid Mg_3Sb_2 is a semiconductor [10].

Liquid Mg_3Bi_2 is a classical example of a liquid semiconductor [11–13] with a conductivity as low as 45 Ω^{-1} cm^{-1}. This is remarkable as so drastic a metal–nonmetal transition in this direction (the solid is a metal and the liquid a semiconductor) had not been observed before (indeed negative changes in the conductivity upon melting occur for most NFE metals and alloys and, e.g., for Te–chalcogenide alloys, but the magnitude of the jump is much smaller in these cases). Also liquid Mg_3Sb_2 is a semiconductor [14, 15]. Plotted as a function of composition the resistivities of liquid Mg–Bi and Mg–Sb exhibit extremely sharp peaks at the octet composition. Measurements of the Darken stability function of Mg–Bi [16, 17] confirm the formation of a very stable and well-defined liquid octet compound.

Xu *et al* [9] extended the measurements of the resistivity of Mg_3Bi_2 beyond the temperature range covered by Grube *et al* to just above the melting point. They found a sudden, small, decrease of the conductivity at the transition from the α- to the β-phase and a much larger jump at the melting point. The conductivity values in between the α–β transition temperature and the melting point correspond to metallic conductivity, but their temperature dependence reminds one of a semiconductor with a very narrow gap. It should be noted that due to experimental problems the actual value of the resistivity measured by Xu *et al* in the liquid is considerably higher than that of [11], but this does not put in question the general nature of the transition at the melting point.

As Mg_3Sb_2 is a semiconductor in both the liquid and the solid state, one expects the Bi atoms, prone to relativistic effects, to be responsible for the peculiar behaviour of solid Mg_3Bi_2. Indeed, a comparative study of the band structures of Mg_3Bi_2 and Mg_3Sb_2 shows that relativistic effects tend to increase metallicity, but cannot account for the whole effect [9]. It has also been conjectured that the liquid state is more favourable for the development of an ionic gap than the solid state, as the irregular coordination in the latter may result in a small Madelung energy. Interestingly, although the electronegativity difference between Mg and Bi is not large, diffraction data [18, 19] indicate a strong, Coulomb-type, ordering in the liquid, particularly at the octet composition.

In the present paper an effort is made to achieve a better understanding of the liquid phase of the Mg–Bi alloy system by means of simulations where the underlying electronic structure of the system is taken into account. To this end we employ the first-principles molecular dynamics (FPMD) approach introduced by Car and Parrinello [20] which has already been successfully applied to the study of numerous liquid and amorphous systems (for a recent review, see [21]). A distinctive feature of the FPMD is that forces between the atoms are calculated directly from the instantaneous electronic ground state. This ground state is calculated via density functional theory in the local density approximation (LDA).

This paper is organized as follows. After presenting the details of the simulation (section 2), in section 3 we deal with the pure Mg and Bi liquids. The atomic and electronic structures of the stoichiometric Mg_3Bi_2 alloy are examined in section 4, while the Mg-rich alloy $Mg_{62}Bi_{28}$ is discussed briefly in section 5. Concluding remarks are given in section 6.

2. Calculations

Calculations were carried out using a periodically repeated simple cubic box containing 90 atoms (e.g. 36 Bi and 54 Mg atoms, in the case of Mg_3Bi_2) [22], except for the case of pure liquid Bi, for which a box with 60 atoms was used. All our simulations were performed at constant volume, which was chosen so as to match the experimental density at the simulation temperature. The electronic states were sampled at the Γ point only, and expanded in plane waves with a kinetic energy cut-off of 12 Ryd. The cut-off for the pseudocharge density was 24 Ryd. Norm-conserving pseudopotentials (NCPP) were used to describe electron–ion interactions. All the final results presented in the following sections were obtained using NCPP constructed by Filippetti and Bachelet (FP) [23], so as to satisfy, besides norm conservation, also the criterion of 'chemical hardness' (see [24]). These pseudopotentials have a [Ne] and a $[Xe]4f^{14}5d^{10}$ core for Mg and Bi respectively, and incorporate 'non-linear core corrections' [25]. The core densities were smoothed by us within a radius r_{smooth} (1.60 au for Mg and 1.98 au for Bi). In the calculations the pseudopotentials were used in the separable form of Kleinman and Bylander (see [26, 27]).

The equations of motion were integrated using the scheme of preconditioning of the wave-function masses according to [28], with a time step between 13 and 15 au, depending on the particular system. During the runs the Kohn–Sham wave functions were kept close to the ground state usually by means of a Nosé thermostat [29–31]. This thermostat compensates for the heat flow, coming from the ionic degrees of freedom, into the fictitious electronic degrees of freedom. To compensate for the drain of energy from the ionic degrees of freedom two Nosé thermostats were employed acting on Mg and Bi ions separately.

In the simulation of the Mg–Bi alloys, the large ratio of the masses of Bi (208.9804 amu) and Mg (24.305 amu) causes the Bi atoms to move rather slowly w.r.t. to the Mg atoms. Consequently very long simulation (CPU) times are needed to obtain reliable statistics. To get around this problem we have chosen to set the Bi mass equal to 30 amu. As a consequence time-dependent properties cannot be calculated reliably any longer, but time-independent properties are not affected.

The constant of motion, i.e. the sum of all energies, which should remain constant during the runs, exhibited quite large fluctuations (about 1/20th of the fluctuations of the potential energy) when the FP potential for Bi was used. This turned out to be related to an insufficient smoothing of the core pseudocharge density of Bi. However, since two parallel runs for pure liquid Bi, one with Bachelet–Hamann–Schlüter (BHS) [53] and the other with FP pseudopotentials, were found to yield substantially identical results (see below), we believe that these fluctuations are not harmful.

Some tests of the pseudopotentials were carried out. These are briefly discussed in the next few paragraphs. A more detailed description can be found in [32]. First we considered the Mg dimer. With 12 Ryd cut-off a ground-state equilibrium distance of 6.50 au and ground-state frequency of 102 cm^{-1} are obtained. The experimental values are 7.35 au and 51 cm^{-1} [33]. The significant underestimation of the distance is known to be related to an inadequate description of the van der Waals interaction between the closed Mg 3s shells by the LDA (see, e.g., [34], for a detailed discussion). However, for larger, i.e. more metallic, systems the van der Waals interaction is less important and a better performance of the LDA is to be expected. Indeed, for bulk hcp Mg Chou and Cohen [35], employing an LDA method, find the lattice constant to agree with experiment within 2%.

To test the Mg pseudopotential in an ionic environment the linear $MgCl_2$ molecule was considered. For Cl a standard BHS pseudopotential was used. For Mg, apart from the FP pseudopotential, tests with the BHS potentials were also carried out. With a p

reference the BHS pseudopotential performs remarkably well, the calculated Mg–Cl distance being $d = 4.11$ au, against an experimental value of 4.12 au [54]. However, with a d reference, which is supposed to provide a more accurate description, the Mg–Cl distance is underestimated by about 8%. With the FP pseudopotential the agreement with experiment is reasonable also with a d reference: $d = 3.99$ au. For this reason this potential was chosen for our final runs.

Also we performed tests on the Bi pseudopotential, and considered in particular the Bi dimer. The experimental ground-state equilibrium distance and frequency are 5.03 au and 173 cm^{-1} respectively. The corresponding computed quantities with a 12 Ryd cut-off are 4.98 au and 165 cm^{-1} respectively [33]. Unfortunately there is not sufficient experimental data available on binary Bi clusters with singlet ground states to allow for a meaningful test of the Bi potential in an ionic environment.

2.1. Details of the simulations

2.1.1. Liquid Mg_3Bi_2. The liquid Mg_3Bi_2 sample consists of 54 Mg and 36 Bi atoms in a periodically repeated simple cubic box. Experimentally the density of Mg_3Bi_2 at 1105 K is 5.465 g cm^{-2} [36]. This yields a length of the cubic box of 26.26 au. Assuming a linear expansion of the volume with temperature, at 1123 K—the temperature of the neutron scattering experiment by Weber *et al* [18]—a length of 26.41 au is obtained. This is the box dimension that we used in our simulations at 1150 K. To justify the procedure described, notice that in [37] the temperature dependence of the volume is found to be almost linear for the related liquid Mg–Sb. Unfortunately the Mg_3Sb_2 composition could not be measured by the authors of [37].

The simulation was started from a slightly deformed lattice with the structure of α-Mg_3Bi_2. We use the conventions from [9] (see, e.g., figure 8 thereof). The 120° angle between the lines connecting the Mg(1) in the xy plane was slightly changed until a larger orthorhombic unit cell containing 3×3 formula units fitted on the lattice. We took two layers (in the direction of the z axis) of these orthorhombic units and expanded them, by different factors for x, y and z direction, to arrive at a cubic cell with the proper density.

Initially we used BHS potentials with a p and a d reference for Mg and Bi respectively. Starting from a temperature close to 2000 K, we slowly cooled the system to a temperature of 1150 K in about 20 000 steps (time step: 13.5 au). At 1150 K the Nosé particles masses were 1 104 000 and 736 000 au for Mg and Bi respectively. The electronic Nosé mass was 48 au. Next we continued for 2680 steps with the FP potential for Mg, but still with the BHS potential for Bi. From this point a d reference was used for both Bi and Mg. The agreement with experiment got worse and we decided to use the FP potentials for both Bi and Mg. We continued for another 17 300 steps. Of these the last 10 000 steps were used to obtain the definitive results.

2.1.2. Liquid Mg, Bi, and $Mg_{62}Bi_{28}$. Shorter simulations of pure liquid Mg, liquid Bi and the liquid alloy $Mg_{62}Bi_{28}$ were carried out also.

For liquid Mg, the initial configuration was obtained from a configuration taken from the Mg_3Bi_2 simulation. All of the Bi were replaced by Mg and the positions were homogeneously rescaled to fit into a box of $(13.43\ \text{Å})^3$, corresponding to the liquid density at 1000 K that we obtained by interpolating between the densities given by Waseda [38]. The 90-atom sample was heated to about 1400 K and then cooled down to a temperature of 1000 K. The equilibration period lasted for 2.9 ps (8100 steps) . The production run lasted for 1.8 ps (5000 steps).

For liquid Bi we took the positions from the same Mg_3Bi_2 configuration as for liquid Mg. Since a simulation with 90 atoms, each having five valence electrons, is computationally quite demanding, we reduced the number of atoms by a cut through the simulation box. We put the remaining 60 atoms in a cubic box of (12.76 Å)^3, corresponding to the density at 573 K according to Waseda [38]. We kept an ionic mass of 30 amu. Whenever below we refer to times for the monatomic liquid Bi system, we correct for this artificial atomic mass, i.e. the time is multiplied by a factor $\sqrt{209/30}$ such as to refer to atoms with 209 amu mass. We started equilibration of the liquid at 1000 K. Originally we intended to carry out the simulation near the experimental melting point of 544 K [3] and therefore chose our simulation box to match the experimental density at 573 K. However, we found that carrying out the simulation at a temperature lower than 1000 K would slow down the diffusion of the atoms so much that the computational effort would become very large. Thus we have finally chosen a simulation temperature of 1000 K. The error this introduces in the length of our box is only 2%. We started 2750 steps (2.28 ps) using the standard BHS potential. Then we switched to the FP potential, i.e. the potential that we also used to obtain our results for liquid Mg_3Bi_2. Equilibration was continued for another 1500 steps with the FP potential. The final averages were obtained from the last 5000 steps (4.15 ps). As a test we also continued the run with the BHS potential for a while and obtained the structure factor and pair distribution function as an average over only 3000 steps. The results obtained with the FP and standard BHS potentials were found to be substantially identical within the limited statics.

For the short simulation of the liquid $Mg_{62}Bi_{28}$ alloy we took a configuration from the simulation of Mg_3Bi_2, subsequently replaced some Bi by Mg atoms and rescaled the positions such as to fit into a box of (13.78 Å)^3. This corresponds to the experimental density at 1100 K [36].

After a short equilibration, averages were calculated over a run of 8000 steps (time step: 13.5 au), where the ionic thermostats operated at a temperature of 1100 K.

3. The pure Mg and Bi liquids

In this section we discuss briefly some properties of the pure Mg and Bi liquids. A more detailed description can be found in [32], while a discussion focusing in particular on electron–ion correlation functions will be presented elsewhere.

3.1. Mg

Figure 1(a) depicts the Mg structure factor and compares it to experiment at 953 K [38]. In figure 1(b) the comparison in real space is made. Agreement between theory and experiment is good. Integrating $g(r)$ to 4.3 Å a coordination number of 12.2 is extracted , a value typical for a hard-sphere-like system. Also the bond-angle distribution (not shown) looks rather hard-sphere-like. This picture is further confirmed by the velocity autocorrelation function (not shown) which shows a clear 'caging' effect. We omit a discussion of the electronic properties since the small size of the periodically repeated cell in conjunction with a sampling at the Γ point only does not allow for a realistic description of, e.g., the density of states of a nearly-free-electron (NFE) metal like Mg.

3.2. Bi

Arsenic, antimony and bismuth all crystallize in a rhombohedral structure [39], i.e. a Peierls distortion of a simple cubic lattice with two atoms per unit cell. The Peierls distortion

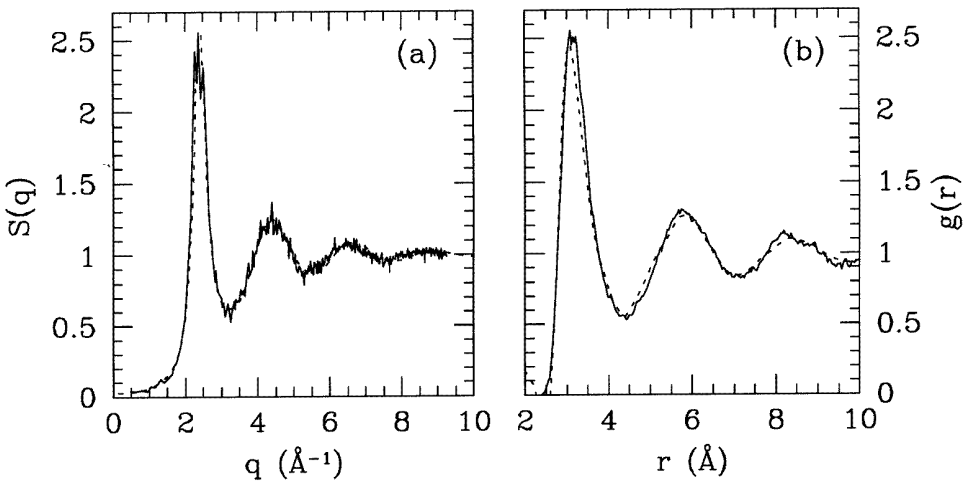

Figure 1. The static structure factor (a) and pair distribution function (b) of liquid Mg obtained by simulation at 1000 K (solid line) compared to experiment at 953 K (dashed line) [38].

causes a splitting of the first coordination shell into two shells containing three atoms each. An atom, together with its three nearest neighbours, forms a flattened tetrahedron. This Peierls distortion is weaker for the heavier elements: for As the two nearest coordination shells are located at 2.9 and 3.5 Å, whereas for Bi they are at 3.1 and 3.5 Å.

The issue of the existence of a structure equivalent to a Peierls distortion in the liquid state was addressed by Hafner and Jank [40] for liquid As, Sb and Bi and by Li [41] for liquid As. Li found by means of an FPMD simulation that liquid As still exhibits structural features in common with the solid. These suggest that a distortion very similar to a Peierls distortion should occur in the liquid: for instance, Li found that liquid As is essentially a threefold-coordinated liquid with bond angles similar to those of the rhombohedral crystal. Our results indicate that for liquid Bi there still are similarities with the rhombohedral lattice, but that these are much less pronounced than for liquid As.

In figure 2(a) we compare the structure factor as obtained from the simulation at 1000 K to the experimental structure factors by Knoll *et al* [42] and Waseda [38] at 923 and 1073 K respectively. In the region of the main peak our data are rather noisy. A small shift of this peak w.r.t. experiment is observed. The overall agreement between experiment and simulation is good.

In figure 2(b) the pair distribution function $g(r)$ is compared to the experimental results [42, 38]. The position of the nearest-neighbour peak in $g(r)$ is well reproduced. The height of this peak, however, is larger than the height of the experimental peak. A similar situation arose for liquid As, where Li [41] showed that the discrepancy could be removed by accounting for the finite q-range accessible to experiment. This was accomplished by broadening the simulation result with the experimental resolution according to a prescription by Etherington *et al* [43]. We used the same procedure for Bi. From figure 2(c) it is apparent that for Bi the discrepancy in the height of the main peak has almost completely vanished. By integration of $g(r)$ the following coordination numbers are extracted: 2.6, 4.8, 6.2 and 7.9 for cut-offs of 3.25, 3.5, 3.75 and 4 Å respectively. From these values and figure 2 it clearly transpires that the number of atoms within the first coordination shell is larger than three. In figure 2(b) the $g(r)$ as obtained from our short test with the BHS potential is also

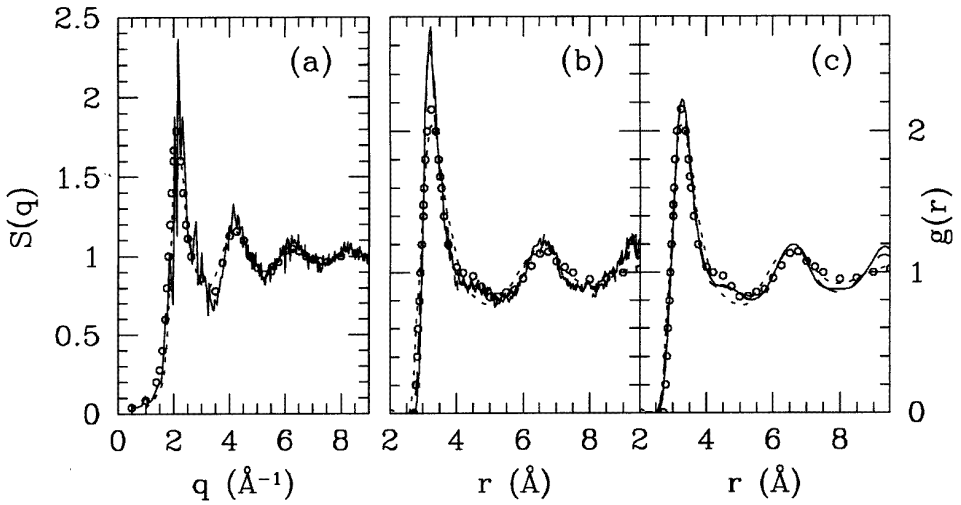

Figure 2. The structure factor (a) and radial distribution function ((b), (c)) of liquid Bi. Solid line: simulation (1000 K); short-dash line: experiment by Waseda [38] (1073 K); circles: experiment by Knoll *et al* [42] at (923 K); long-dash line: short test calculation with the BHS pseudopotential ($g(r)$ only). Note that (b) shows the 'raw' simulation data, while (c) shows the simulation data broadened with the resolution of Knoll's experiment (12 $Å^{-1}$) according to a prescription by Etherington *et al* [43]. The broadening was carried out in real space by means of a convolution.

plotted. It is essentially the same as the $g(r)$ obtained with the FP pseudopotential.

Figure 3 depicts the bond-angle distribution. For decreasing interatomic distances it changes significantly and becomes quite similar to the bond-angle distribution of the crystal.

The electronic density of states (DOS), obtained by averaging over three configurations sampled at 2000 step intervals, has a clear metallic character (see figure 4). The angular momentum decomposition is obtained by projecting on spherical harmonics in a sphere with radius 3 au. The s–p splitting is evident. The liquid-state DOS was also calculated by Hafner and Jank [40]. Their DOS and ours are similar, the s part being a little broader in our case. The DC conductivity extrapolated from $\sigma(\omega)$ is about 3 $m\Omega^{-1}$ cm^{-1}. $\sigma(\omega)$ is calculated from the Kubo–Greenwood formula [44] with the electrons distributed according to a Fermi-distribution at 0 K:

$$\sigma(\omega, \{\boldsymbol{R}_I\}) = \frac{2\pi e^2}{3m^2\omega\Omega} \sum_{m}^{occ} \sum_{n}^{unocc} \sum_{\alpha} |\langle\psi_m|\hat{p}_\alpha|\psi_n\rangle|^2 \delta(E_n - E_m - \hbar\omega) \qquad (1)$$

where m and e are electron mass and charge respectively, Ω is the MD cell volume, $\hat{p}_\alpha$ is the α-component of the momentum operator and *occ* and *unocc* denote occupied and unoccupied eigenstates respectively. The experimental DC conductivity at 1173 K is 6.5 $m\Omega^{-1}$ cm^{-1} [11]. In calculations employing density functional theory usually the width of the gap is underestimated and as a result the conductivity is overestimated. In this case, instead, the conductivity is underestimated. This may probably be explained by the neglect of spin–orbit interactions. For rhombohedral Bi, Gonze *et al* [45] (see in particular figure 9 thereof) find a less metallic DOS in the case where the spin–orbit interaction is switched off.

Hafner and Jank [40] have simulated liquid As, Sb and Bi with pair potentials based on second-order perturbation theory. They proposed that the liquid structure is determined by the diameter of the atomic core and the wavelength and amplitude of the Friedel oscillation

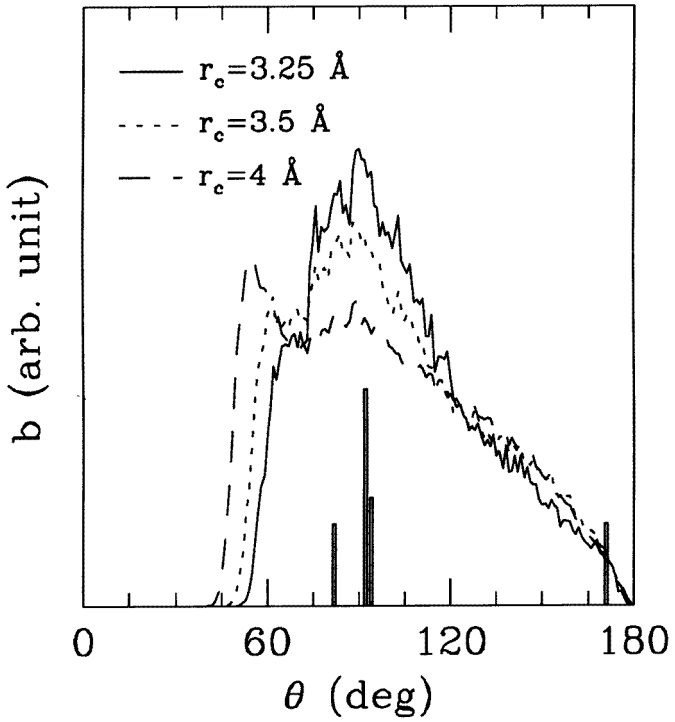

Figure 3. The calculated bond-angle distribution for liquid Bi. Various cut-off lengths (r_c) to define a bond have been employed. The vertical bars are proportional to the bond-angle distribution of rhombohedral Bi [39] within the first two coordination shells at 3.1 and 3.5 Å. Both shells contain three atoms. The third coordination shell is at 4.5 Å. The first shell is responsible for the large peak just beyond 90°.

in the pair potential. They argued that the combined effect of these may stabilize an open structure, thus giving a real-space description of an effect that in the crystal is caused by the Peierls distortion. In their view the relativistic effects cause the amplitude of the Friedel oscillations to decrease, which explains the trend towards a more close-packed liquid structure going from As to Bi. The same trend in the liquid structure is seen from the first-principles simulations when we compare the results on liquid As obtained by Li [41] to those on liquid Bi presented here. A simulation closer to the experimental Bi melting point of 544 K might show, however, more similarities with the rhombohedral crystal.

4. Liquid Mg_3Bi_2

4.1. Structural properties

Figure 5(a) shows the static structure factor, according to the Faber–Ziman definition, of liquid Mg_3Bi_2, obtained from experiment [18] and from our simulation. The overall agreement is quite good. There are some small differences—e.g., the shoulder in front of the main peak is lower in the simulation.

The comparison between experiment and simulation in real space is presented in figure 5(b). Here $D(r) = 4\pi r\rho_0(g(r) - 1)$, where ρ_0 is the number density and $g(r)$ the

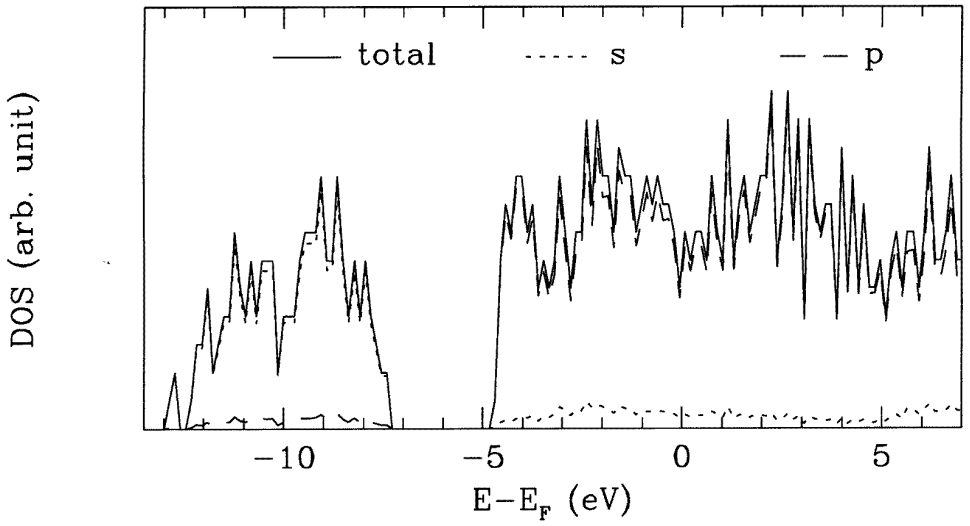

Figure 4. The electronic density of states for liquid Bi. Dotted line: s; dashed line: p; solid line: total.

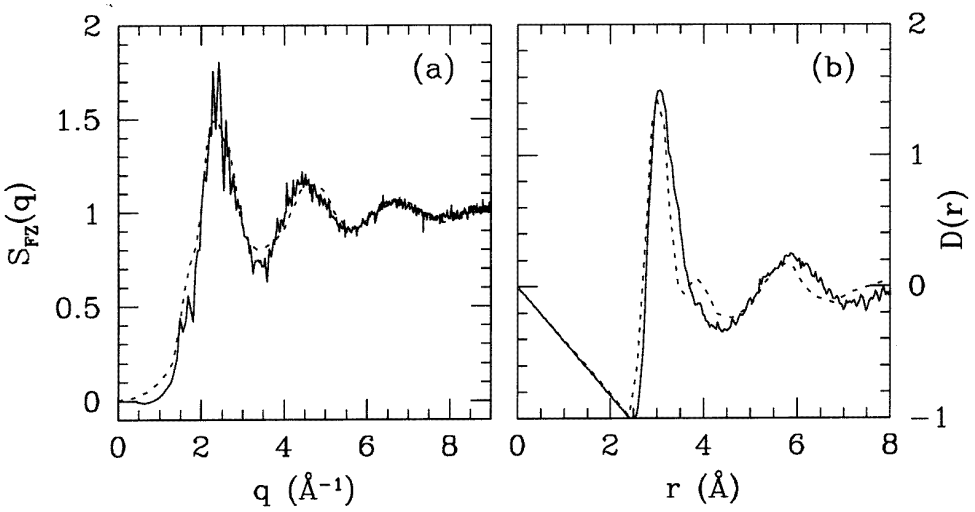

Figure 5. The static structure factor according to the Faber–Ziman definition (a) and $D(r)$ (b) of liquid Mg_3Bi_2. Continuous line: simulation at 1150 K; dotted line: experiment at 1123 K from [18].

conventional pair distribution function, is plotted. The height and left-hand side of the main peak follow the experiment very well. The main peak, however, is too broad and the small hump just beyond the main peak in the experiment is not reproduced. This discrepancy cannot be traced back to a specific feature of the partial pair distribution functions (g_{ij}, figure 6). It might originate from either g_{BiBi}, g_{MgMg} or a complicated mix of all three partial g_{ij}.

The partial structure factors (S_{ij}, Ashcroft–Langreth definition) are displayed in figure 7.

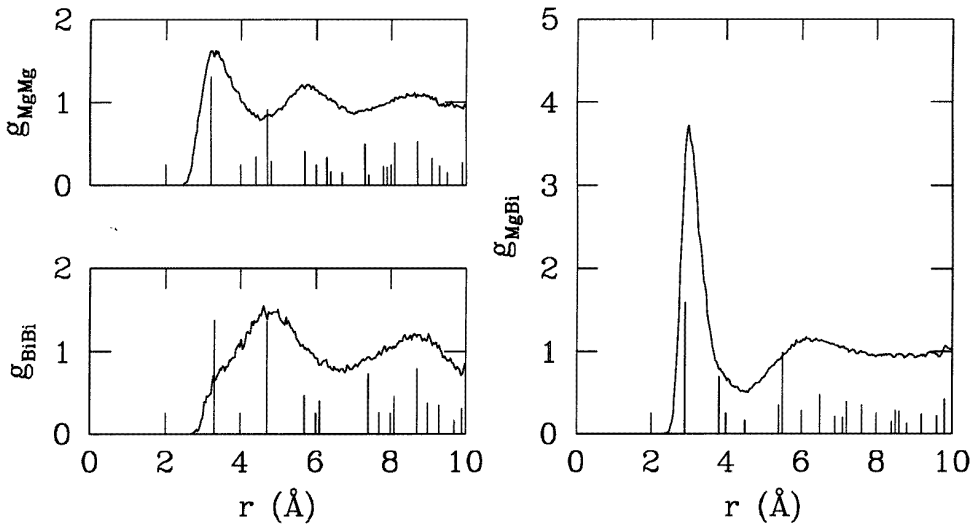

Figure 6. Partial pair distribution functions of liquid Mg_3Bi_2. The vertical bars are proportional to the g_{ij} of the crystalline α-phase.

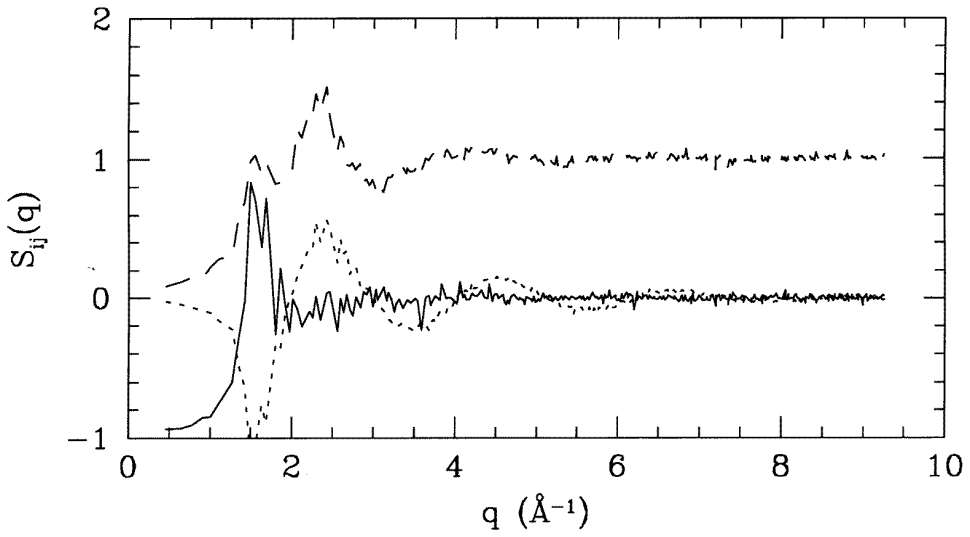

Figure 7. Partial structure factors of liquid Mg_3Bi_2 according to the Ashcroft–Langreth definition. $S_{BiBi} - 1$: continuous line; S_{MgBi}: dotted line; S_{MgMg}: dashed line.

There are clear features of an ionic ordering. The wiggles in S_{BiBi} and S_{MgMg} decay much more rapidly than those in S_{MgBi}. In direct space this is mirrored by the sharpness of the main peak of g_{MgBi}. This peak is located at 3 Å. Since the position of the main peaks of $g(r)$ and $S(q)$ (r_P and q_P) are approximately related by $r_P = 7.7/q_P$ [46], the main peak of S_{MgBi} is expected to occur at approximately $7.7/3 = 2.57$. Indeed the main peak in S_{MgBi} is found close to 2.5. However, a negative prepeak occurs at 1.5 Å^{-1}, which we consider to be the strongest indication for an ionic ordering. The low degree of structure in S_{MgMg}

and, even more so, in S_{BiBi} is clearly mirrored by the absence of sharp peaks in g_{MgMg} and g_{BiBi}. Also S_{BiBi} and S_{MgMg} have peaks at ≈ 1.5 Å^{-1}. In the case of S_{MgMg} this peak can also be interpreted as a prepeak: the first maximum in g_{MgMg}, at 3.3 Å, corresponds to the main peak in S_{MgMg} which is located at approximately 2.4 Å^{-1}. For S_{BiBi} the peak at 1.5 Å^{-1} also indicates a superstructure. However, it corresponds with the main, and first, top of g_{BiBi}: $7.7/1.5 = 5.1$ Å. The peaks at 1.5 Å^{-1} interfere in such a way that their only remnant in the total neutron $S(q)$ is the shoulder on the left-hand side of the main peak of the total $S(q)$, clearly visible in the experimental results and marginally in MD results.

Whereas the g_{BiBi} and g_{MgMg} have their main peaks at rather different interatomic separations, the shortest Mg–Mg and Bi–Bi distances are approximately the same (figure 6). Moreover g_{BiBi} has a shoulder where g_{MgMg} has its main maximum. So the conclusion that Bi and Mg are of similar size is justified, supporting the interpretation of the main peak of g_{BiBi} as a superstructure feature. The first coordination shell around a Bi atom should contain mainly Mg atoms.

The differences between Mg–Mg and Bi–Bi correlations are of course largely determined by the concentration difference and, consequently, the charge difference. Most clearly the consequences, and the differences w.r.t. the crystalline α-phase, are recognized by considering the partial running coordination numbers $a_{ij}(r)$, i.e. the number of atoms of species i that on average are within a shell of radius r around an atom of type j (figure 8). From the $a_{ij}(r)$ it transpires that the 'shell' of atoms around a Bi atom consists predominantly of Mg atoms. Certainly below 4 Å the ratio of the number of Mg atoms around a Bi atom to the number of Bi atoms around a Bi atom is much larger than 3/2, the number to be expected for a homogeneous mixture of neutral, equally sized, particles.

Next we compare our liquid with the crystal structure of the α-phase [6]. The height of the 'spikes' in figure 6 is proportional to the crystalline $g_{ij}(r)$. In particular when comparing these to the liquid state g_{BiBi} and g_{MgBi} it emerges that the crystalline structure does not fit very well to the liquid-state structure. In the α-phase the Bi atoms approach closely. When going to the liquid phase, the Bi atoms move apart (clearly illustrated by a_{BiBi}), consistently with the ionic nature of the liquid.

Some of the bond-angle distributions (b) are presented in figure 9. The shape of the g_{ij} (figure 6), and even more so the shape of the a_{ij} (figure 8) clearly show that a definition of a cut-off on the bond length, especially for Bi–Bi bonds, is problematic. We rather arbitrarily took a value of 4 Å. Together with the liquid-state bond-angle distributions, those for the α-phase are also shown. In comparing the distributions of the two phases one should keep in mind the $\cos(\theta)$ background that, on purely statistical grounds, is present in the liquid. The occurrence of a peak at 60° in b_{MgMgMg} shows that in the liquid state the Mg atoms are much more closely packed. b_{BiBiBi} indicates a slight preference for the 90° angle also found in the crystal. We checked that decreasing the cut-off to 3.5 Å does not bring out this feature more clearly. For the 5 Å cut-off it is washed out already.

4.2. Electronic properties

Figure 10 shows the electronic density of states (DOS) obtained from our simulation. The DOS was obtained as an average over five configurations at 2000 step intervals. The self-consistent potential (Hartree and exchange–correlation terms) from the liquid simulation was used to construct a proportion of the unoccupied eigenstates. In turn, these were used to calculate the DOS and the frequency-dependent conductivity. The DOS does not have a gap at the Fermi level; it even looks rather metallic. We come back to this point below.

The Bi s levels are clearly split off from the Bi p levels. This is a situation similar to

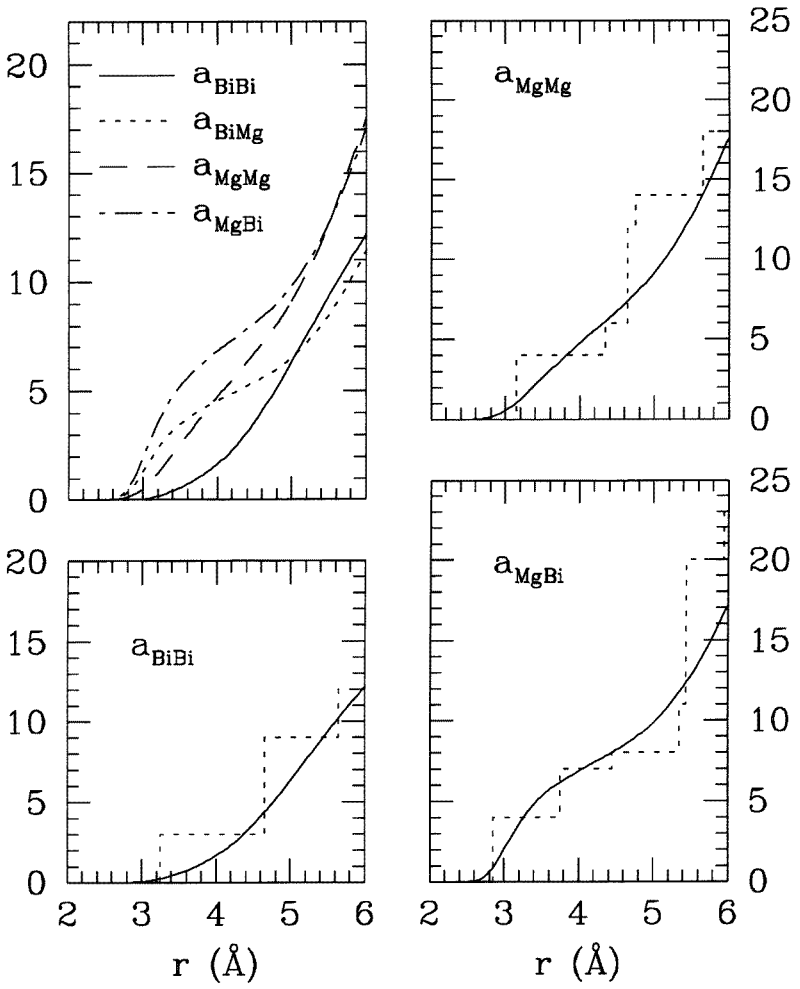

Figure 8. Partial $a_{ij}(r)$: the number of atoms of species i that on average are within a shell of radius r around an atom of type j. The dotted 'step-like' functions are the a_{ij} of the α-phase. The crystalline data are taken from [6, 9].

that encountered in, e.g., liquid Pb where scalar relativistic effects push down the s levels [49]. The same was observed in the band-structure calculations of crystalline α-Mg_3Bi_2 by Xu *et al* [9] where the mass–velocity and Darwin terms push down the s levels from above -10 eV to below -10 eV. Comparing to the scalar relativistic band structure in [9] we see that the main effect of going from the crystal to the liquid phase is to 'broaden' these low-lying bands such that they come closer to the Mg and Bi p levels.

The projections to obtain an angular momentum decomposition of the DOS were carried out in spheres of 3 au radius centred on the nuclei. If we renormalize the DOS in these spheres we find that on average almost one electron has been transferred to a Bi atom. Of course this number is very approximate, but since Mg and Bi are of similar size it clearly demonstrates the direction and order of magnitude of the charge transfer, lending support to the ionic picture.

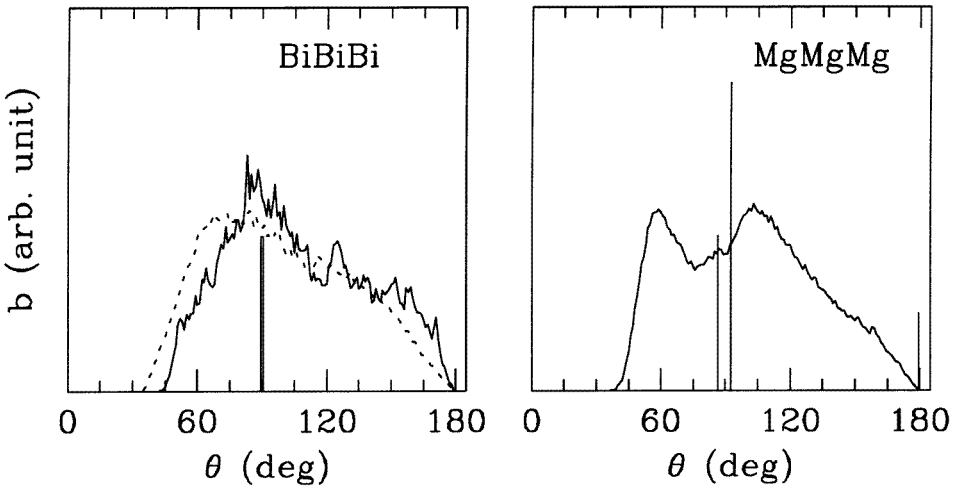

Figure 9. Bi–Bi–Bi and Mg–Mg–Mg bond-angle distributions for liquid Mg_3Bi_2. For the solid lines the cut-offs are 4 Å. The dotted line pertains to a cut-off of 5 Å on Bi–Bi distances. The heights of the vertical lines are proportional to the bond-angle distribution of the α-phase, the cut-offs being also 4 Å.

$\sigma(\omega)$ was calculated from the Kubo–Greenwood formula [44], with the electrons distributed according to a Fermi distribution at a temperature of 0 K (equation (1)). The extrapolation to zero frequency (≈ 2 mΩ^{-1} cm^{-1}) should be considered with care because of the poor statistical quality (only a few transitions) and the extremely narrow energy range where temperature effects become important ($k_{\mathrm{Boltz}}T = 0.1$ eV at 1150 K). However, it is apparent that we significantly overestimate the DC conductivity—that from the best of the available experiments is found to be a mere 45 Ω^{-1} cm^{-1}.

Looking for possible reasons for this discrepancy between simulation and experiment, we consider first the experimental side. The resistivity maximum is reached in an extremely narrow composition range (see, e.g., figure 7 of [9]). Problems because of an insufficient chemical definitions of the sample may arise.

Next we consider some possibilities from the theoretical side. (i) It is not plausible that the quality of the pseudopotentials is insufficient. From the comparison with diffraction experiments it has become clear that they describe a system that rather closely approaches the structure of the true liquid. (ii) We used scalar relativistic pseudopotentials; the $\boldsymbol{L} \cdot \boldsymbol{S}$ term was ignored. For crystalline α-Mg_3Bi_2 [9] shows that inclusion of spin–orbit coupling enhances the metallic behaviour. So inclusion of the $\boldsymbol{L} \cdot \boldsymbol{S}$ term will probably enhance the conductivity, rather than decreasing it. (iii) This leaves us with the most obvious source of trouble: density functional theory, which generally tends to underestimate the energy separation between occupied and unoccupied states, even when the local density approximation is relaxed [51].

5. The $Mg_{62}Bi_{28}$ alloy

In figure 12 the neutron structure factor and $D(r)$, as obtained from the simulation of $Mg_{62}Bi_{28}$ (i.e. $Mg_{0.689}Bi_{0.311}$), are compared to the experimental results by Weber *et al* [18] for the $Mg_{70}Bi_{30}$ alloy at 980 K. The overall agreement for the $S(q)$ is satisfactory; only

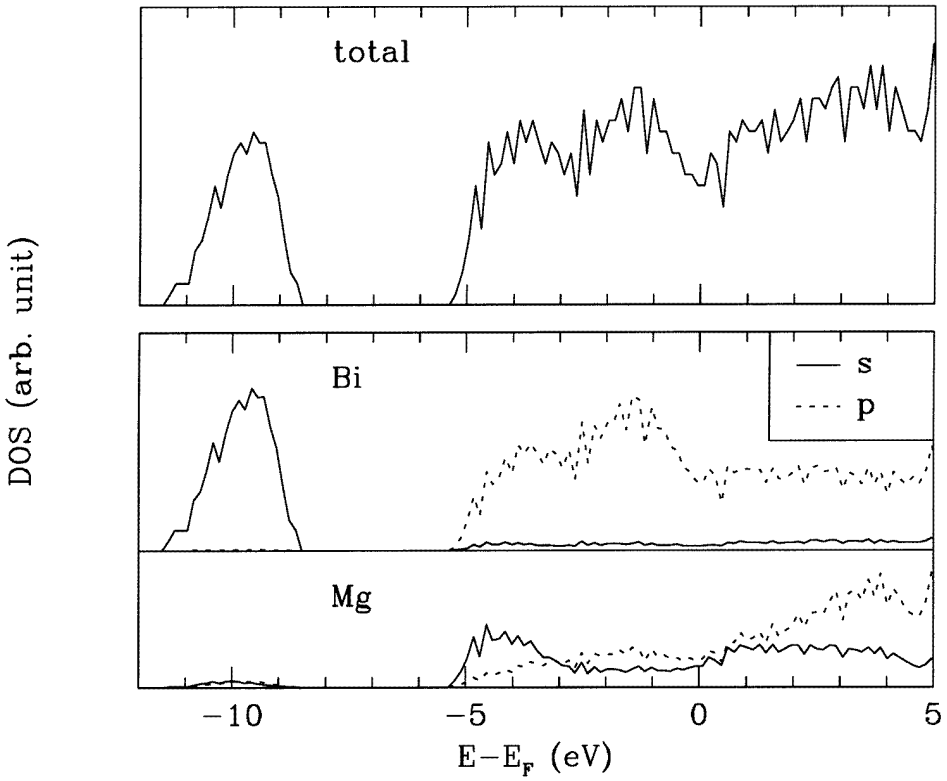

Figure 10. The electronic density of states of liquid Mg_3Bi_2, obtained as an average over five configurations at 2000 step intervals. The upper panel displays the total DOS. The lower panels display a decomposition into chemical species and angular momentum where the decomposition was obtained by projecting on spherical waves of the appropriate symmetry in a sphere with a radius of 3 au.

at larger wavenumbers is some shift apparent. The main peak of $D(r)$ is slightly shifted w.r.t. experiment. The hump in $D(r)$ at ≈ 4.7 Å is not reproduced in the simulation. In the simulation the next hump develops into a broad maximum at 6 Å.

Comparing the simulation results at the two alloy compositions, we notice that they are much more similar than the experimental results. Within the noise, the only discernible difference in the calculated $S(q)$ is the height of the main peak, which is slightly larger for the Mg-richest alloy. On comparison of the theoretical $D(r)$ curves the only clear difference is that for the Mg-rich alloy the maximum is slightly more pronounced (but does not shift). In the experimental data the same trend is observed, but also other peaks vanish or come into existence.

From the partial pair distribution functions (not shown), we find that some Mg atoms have moved into the first coordination shell of Mg at the expense of some Bi atoms. The number of atoms around a Bi atom decreased by about 0.5 (for a wide range of cut-offs) whereas the maximum increase of the number of atoms around a Mg atom is about 0.7. This change in coordination number is not so pronounced as that inferred by Weber *et al* from their experimental data. The prepeak in S_{MgMg} (not shown) is reduced to a very weak shoulder on the side of the main peak (which becomes a little higher). The absolute height

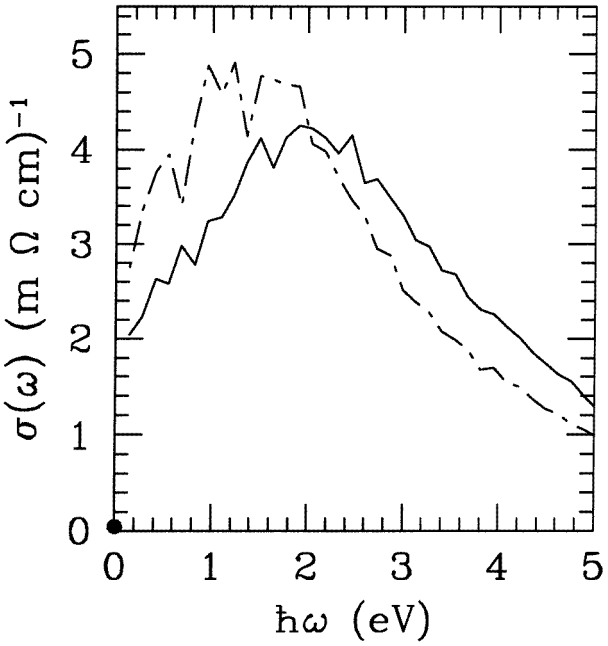

Figure 11. The frequency-dependent conductivity. The solid line pertains to Mg_3Bi_2 and is calculated as an average over five independent configurations. The solid circle corresponds to the measured DC conductivity of Mg_3Bi_2 from [11]. The dash–dotted line pertains to $Mg_{62}Bi_{28}$ and was obtained as an average over four configurations.

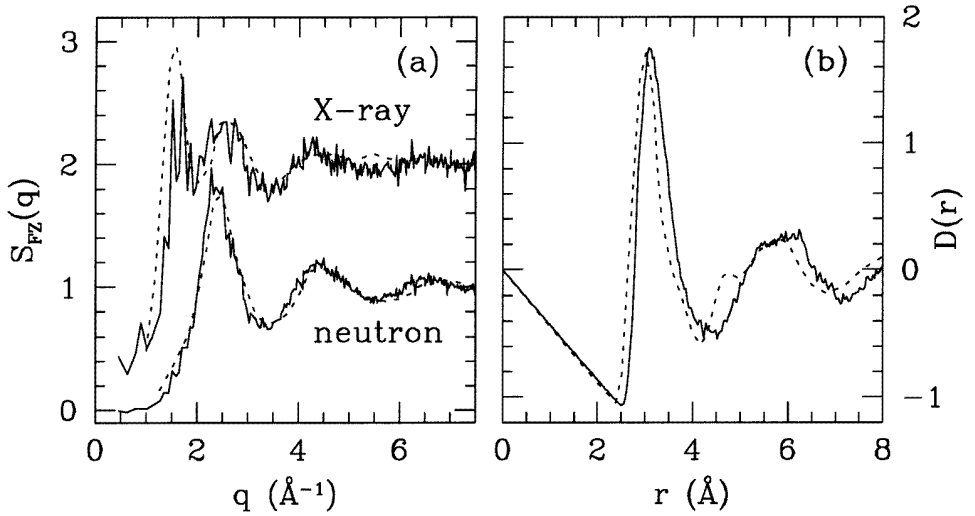

Figure 12. Neutron and x-ray structure factors (a) and $D(r)$ (b) of liquid $Mg_{62}Bi_{28}$. Solid lines: simulation ($Mg_{62}Bi_{28}$); dotted lines: experiment (Mg_7Bi_3), [18].

of the prepeak of S_{MgBi} is a little reduced. The bond-angle distributions are very similar to those of the Mg_3Bi_2 alloy.

The trend in the structure when going from Mg_3Bi_2 to $Mg_{62}Bi_{28}$ is not surprising: the number of Bi atoms is reduced w.r.t. the number of Mg atoms, so Mg moves into the first coordination shell of Mg at the expense of Bi. This causes a reduction of the size of the S_{MgMg} and S_{MgBi} prepeaks, without really affecting the typical length scale of the liquid superstructure. However, the subtle changes in the experimental $S(q)$ and $D(r)$ are not found in the simulation.

Weber *et al* also carried out x-ray diffraction measurements on the Mg_7Bi_3 alloy. In figure 12(a) we compare their x-ray structure factor and the structure factor obtained by taking the appropriate mixture of the partial structure factors from our simulation and the atomic form factors (taken from [50]). Note that the height of the first peak is somewhat underestimated. This peak consists of a positive Bi–Bi and a negative Mg–Bi contribution. (The contributions from the Mg–Mg partial are negligibly small). The wiggles beyond the first peak originate almost entirely from the Mg–Bi partial, whereas the noise comes from the unstructured Bi–Bi partial.

The electronic density of states of $Mg_{62}Bi_{28}$ (not shown) is very similar in character to the DOS of the Mg_3Bi_2 liquid, i.e. there is no gap at E_{Fermi}. The conductivity as a function of ω is shown in figure 11. It was obtained by averaging over four configurations only, and thus the quality of the statistics is not very good, especially for the lower frequencies. The extrapolated DC value is similar to that obtained for the Mg_3Bi_2 alloy. Its value is in between the experimental conductivities at the $Mg_{0.74}Bi_{0.26}$ and the $Mg_{0.62}Bi_{0.38}$ compositions, which are respectively ≈ 3.0 and 1.5 $m\Omega^{-1}$ cm^{-1} [11–13]. Therefore comparison with experiment is satisfactory at this composition.

6. Concluding remarks

Our results show that liquid Mg_3Bi_2 essentially conforms to the simple ionic behaviour to be expected for an octet compound. Mg–Mg close contacts occur quite frequently, simply because Mg is the most abundant species. However, even Bi atoms sometimes penetrate the first coordination shell of a Bi atom. Therefore, in line with the moderate electronegativity difference (0.7 on the Miedema scale [52]), the ionicity is not very large. Essentially it amounts to a screening of the species with highest absolute charge (Bi) by the Mg ions. A physical transfer of charge equal to the formal transfer of charge ($Mg_3^{2+}Bi_2^{3-}$) seems, in view of all the structural data presented, not very realistic. This is in accordance with our rough estimate of about one electron on average being transferred to a Bi atom.

In [9] it was speculated that the unusual sevenfold Mg–Bi coordination, to which the crystalline system is forced by composition and lattice periodicity, could change in the liquid state into a more regular coordination that allows an ionic gap to be formed. From the shape of the partial g_{ij} in figure 5(b) it follows that coordination numbers are difficult to determine. Therefore we used the running coordination numbers (figure 8) to demonstrate that the Mg_3Bi_2 liquid-state structure is not just a trivial modification of the solid-state structure but that distances change, in particular those between Bi atoms, to allow for a more ionic ordering. The structural modifications that we find going from the α-phase to the liquid are consistent with the structure of the superionic β-phase [7] where also an increase in Bi–Bi distance (4.6 Å) is observed.

We could not give a good description of the electronic behaviour near the Fermi level for the Mg_3Bi_2 liquid. However, the resistivity of the $Mg_{62}Bi_{28}$ alloy is in good agreement with experiment. Thus in our calculation the opening of a narrow gap, in a very narrow composition range around the stoichiometric composition, is not realized. Like in numerous other cases the most obvious possible reason for this is the use of density functional theory.

However, this does not rule out the possibility of the occurrence of another mechanism which is beyond the approximations of our calculations.

Acknowledgments

We thank Dr A Filippetti and Dr G B Bachelet for supplying the pseudopotentials.

This work was sponsored by the Srichting Nationale Computerfaciliteiten (National Computing Facilities Foundation, NCF) for the use of supercomputer facilities, with financial support from the Nederlandse Organisatie voor Wetenschappelijk Onderzoek (Netherlands Organization for Scientific Research, NWO).

References

[1] Seitz F 1940 *The Modern Theory of Solids* (New York: McGraw-Hill)
[2] Grube G and Bornhak R 1934 *Z. Elektrochem.* **40** 140
[3] Massalski T B, Murray J L, Bennet L H, Baker H and Kaprzak L 1986 (Metal Park, OH: The American Society for Metals)
[4] Grube G, Mohr L and Bornhak R 1934 *Z. Elektrochem.* **40** 143
[5] Zintl E and Husemann E 1933 *Z. Phys. Chem.* **20** 272
[6] Gottfried C and Schossberger F 1937 *Struct. Rep. (Strukturber. 1933–1935)* **3** 48
[7] Barnes A C, Guo C and Howells W S 1994 *J. Phys.: Condens. Matter* **6** L467
[8] Stepanow N J 1912 *Z. Anorg. Allg. Chem.* **78** 1
[9] Xu R, de Groot R A and van der Lugt W 1993 *J. Phys.: Condens. Matter* **5** 7551
[10] Busch G, Hulliger F and Winkler U 1954 *Helv. Phys. Acta* **27** 249
[11] Enderby J E and Collings E W 1970 *J. Non-Cryst. Solids* **4** 161
[12] Ilscher B R and Wagner C 1958 *Acta Metall.* **6** 712
[13] Glazov V M and Situlina O V 1969 *Akad. Nauk. SSSR Chem.* **167** 587
[14] Verbrugge D M and van Zytveld J B 1993 *J. Non-Cryst. Solids* **156–158** 736
[15] Verbrugge D M and van Zytveld J B 1993 *J. Phys. D: Appl. Phys.* **26** 1722
[16] Egan J J 1959 *Acta Metall.* **7** 560
[17] Darken L S 1967 *Trans. Metall. Soc. AIME* **239** 80
[18] Weber M, Steeb S and Lamparter P 1979 *Z. Naturf.* a **34** 1398
[19] Boos A and Steeb S 1977 *Phys. Lett.* **63A** 333
[20] Car R and Parrinello M 1985 *Phys. Rev. Lett.* **55** 2471
[21] Galli G and Pasquarello A 1993 *First-principles Molecular Dynamics in Computer Simulation in Chemical Physics* ed M P Allen and D J Tildesley (Dordrecht: Kluwer) p 261
[22] Therefore we refer to $Mg_{0.689}Bi_{0.311}$ as $Mg_{62}Bi_{28}$.
[23] Filippetti A and Bachelet G B 1994 Private communication
[24] Teter M 1993 *Phys. Rev.* B **48** 5031
[25] Louie S G, Froyen S and Cohen M L 1982 *Phys. Rev.* B **26** 1738
[26] Kleinman L and Bylander D M 1982 *Phys. Rev. Lett.* **48** 1425
[27] The projections were carried out on the atomic eigenfunctions of the BHS pseudopotentials.
[28] Tassone F, Mauri F and Car R 1994 *Phys. Rev.* B **50** 10 561
[29] Nosé S 1984 *J. Chem. Phys.* **81** 511
[30] Hoover W G 1985 *Phys. Rev.* A **31** 1695
[31] Blöchl P E and Parrinello M 1992 *Phys. Rev.* B **45** 9413
[32] de Wijs G A 1995 *PhD Thesis* Rijksuniversiteit Groningen
For a copy write to the last author.
[33] Huber K P and Herzberg G 1979 *Spectra of Diatomic Molecules (Molecular Spectra and Molecular Structure 4)* (New York: Van Nostrand Reinhold)
[34] Ortiz G and Ballone P 1991 *Phys. Rev.* B **43** 6376
[35] Chou M Y and Cohen M L 1986 *Solid State Commun.* **57** 785
[36] Faxon R C 1966 *PhD Thesis* Syracuse University
[37] Hansen A R, Kaminski M A and Eckert C A 1990 *J. Chem. Eng. Data* **35** 153
[38] Waseda Y 1980 *The Structure of Non-crystalline Materials* (New York: McGraw-Hill)
[39] Ashcroft N W and Mermin N D 1988 *Solid State Physics* (New York: Saunders)

[40] Hafner J and Jank W 1992 *Phys. Rev.* B **45** 2739
[41] Li X-P 1990 *Phys. Rev.* B **41** 8392
[42] Knoll W, Lamparter P and Steeb S 1983 *Z. Naturf.* a **38** 395
[43] Etherington G, Wright A C, Wenzel J T, Dore J C, Clarke J H and Sinclair R N 1982 *J. Non-Cryst. Solids* **48** 265
[44] Mott N F and Davis E A 1979 *Electronic Processes in Non-crystalline Materials* (Oxford: Clarendon)
[45] Gonze X, Michenaud J-P and Vigneron J-P 1990 *Phys. Rev.* B **41** 11 827
[46] The real-space periodicity corresponding to the prepeak is $2\pi/q_{\mathrm{P}}$, where q_{P} is the prepeak position. Due to the spherical averaging in the Fourier transform from reciprocal to direct space, the first maximum in the contribution of the prepeak to the pair distribution function will be at approximately $7.7/q_{\mathrm{P}}$. For an extensive review see, e.g., [47].
[47] Salmon P S 1994 *Proc. R. Soc.* A **445** 351
[48] Bhatia A B and Thornton D E 1970 *Phys. Rev.* B **2** 3004
[49] Jank W and Hafner J 1990 *Phys. Rev.* B **41** 1497
[50] 1974 Revised and supplementary tables *International Tables for X-Ray Crystalography* vol IV (Birmingham: Kynoch)
[51] Perdew J and Levy M 1983 *Phys. Rev. Lett.* **51** 1884;
Sham L and Schlüter M 1983 *Phys. Rev. Lett.* **51** 1888
[52] Miedema A R, Boom R and de Boer F R 1975 *J. Less-Common Met.* **41** 283
[53] Bachelet G B, Hamann D R and Schlüter M 1982 *Phys. Rev.* B **26** 4199
[54] Akishin P A and Spiridonov V P 1958 *Kristallografiya* **2** 465